Applied Thermal Engineering 245 (2024) 122801

Contents lists available at ScienceDirect

Applied Thermal Engineering

journal homepage: www.elsevier.com/locate/apthermeng

Research Paper

Monitoring internal heat fluxes on Pulsating Heat Pipes using Kalman filter – Numerical and experimental results

Bruno H.M. Margotto [a], Carlos E.P. Kopperschmidt [a], Marcelo J. Colaço [a,*], Wellington B. da Silva [b], Fabio Bozzoli [c,d], Luca Cattani [c], Luca Pagliarini [c]

[a] Department of Mechanical Engineering, Federal University of Rio de Janeiro, Rio de Janeiro, RJ 21941-972, Brazil
[b] Department of Rural Engineering, Federal University of Espírito Santo, Alegre, ES 29500-000, Brazil
[c] Department of Engineering and Architecture, University of Parma, Parco Area delle Scienze 181/A, Parma, Italy
[d] SITEIA.PARMA Interdepartmental Centre, University of Parma, Parco Area delle Scienze 181/A, Parma, Italy

ARTICLE INFO

Keywords:
Inverse heat conduction problem
Kalman filter
Pulsating Heat Pipe

ABSTRACT

The present study proposes an approach to monitor the wall-to-fluid internal heat flux on Pulsating Heat Pipes (PHP), which provides meaningful information about the efficiency and limiting operation conditions of such devices. In this sense, the current work adopts the Kalman Filter (KF) to estimate the heat flux between the working fluid and the internal tube wall along the adiabatic section of a PHP device by solving an inverse heat conduction problem. The KF is a well-known tracking technique, and therefore the current study is attractive due to the possibility of real-time evaluation of internal heat fluxes, a prospect that is extremely difficult to realize by standard whole domain inverse problem techniques. A high-speed and high-resolution infrared camera performs the temperature acquisition on the external wall of the PHP device. Two mathematical heat conduction models are considered: complete and thin-wall models. The complete model determines the temperature and heat flux evolution over time, and the thin-wall model is used to correct the random walk parameter on the KF formulation. Since the time step needed to the KF evolution model is smaller than the measurements acquisition interval, a matrix manipulation is used during the prediction step, reducing the number of mathematical operations. Hence, instead of predicting the states until reaching the measurement times, a proper mathematical manipulation reduces several mathematical operations to a single one. Then, the KF estimation capability is evaluated by considering synthetic data with different noise levels and different heat flux values. Subsequently, real experimental data are employed, and the results are compared with the ones obtained via a standard whole domain technique. The results obtained with the KF presented good visual agreement with the exact solution. Once the KF presents a delayed response, which is a characteristic of some filtering techniques, the errors with synthetic data were calculated offsetting the delay of the estimation in time in order to make a fair comparison, showing a maximum estimation error lower than 36 % considering the highest noise level. The synthetic data considered 20 s of time experiment, and the KF was able to estimate the PHP internal heat flux in less than 12 s, including the smoothing temperature step, showing fast and accurate results. For the real experimental data, the agreement between the KF and a whole domain technique is highly commendable, demonstrating a deviation of 25.5 % between both techniques. Moreover, the KF required significantly less computational time. The proposed methodology for heat flux estimation on PHPs is promising to evaluate their thermal behavior in real-time due to a low CPU time and computational memory required, as well as its simplicity to be implemented, possibly on embarked devices. Such information may therefore provide a thermal indicator of the correct functioning of PHPs in real time applications.

1. Introduction

Many engineering fields have been subjected to a high rate of development, such as the sustainable energy, electronics, and aerospace areas, among others, reaching the need for a high level of computational power and, consequently, energy generation. On the other hand, this technological advancement increased the necessity of removing higher

* Corresponding author.
E-mail address: colaco@ufrj.br (M.J. Colaço).

https://doi.org/10.1016/j.applthermaleng.2024.122801
Received 13 November 2023; Received in revised form 5 February 2024; Accepted 21 February 2024
Available online 24 February 2024

Nomenclature

c_p	Specific heat at constant pressure, J/kg.K
h_∞	Convection heat transfer coefficient, W/m^2.K
k	Subscript for time step instant
L	Tube length, m
N_{nodes}	Number of nodes of discretization on the measured surface
N_t	Number of predict calculation between two measurements
N_r	Number of nodes in radial direction
N_z	Number of nodes in axial direction
q	Heat flux per unit surface, W/m^2
q_{est}	Estimated heat flux per unit surface, W/m^2
q^{model}	Heat flux from jumped model per unit surface, W/m^2
r	Radial coordinate, m
t	Time, s
T	Temperature, K
T_∞	Environmental temperature, K
z	Axial coordinate, m
$\mathbf{F}$	Evolution matrix for Kalman filter
$\mathbf{F}_{fdm}$	Matrix resulted from the Finite Difference Method
$\mathbf{H}$	Observation matrix for the Kalman filter
$\mathbf{K}$	Gain matrix for the Kalman filter
$\mathbf{P}$	Covariance matrix of state, K^2 or W^2/m^4
$\mathbf{Q}$	Covariance matrix of evolution model for the Kalman filter, K^2
$\mathbf{R}$	Covariance matrix of observation model for the Kalman filter, K^2
$\mathbf{u}$	Input vector for the Kalman filter, K
$\mathbf{x}$	State vector, K or W/m^2
$\mathbf{z}$	Measurement vector, K

Greek Letters

α	Thermal diffusivity, m^2/s
ρ	Density, kg/m^3
Γ_0	Boundary on bottom surface
Γ_{ext}	Boundary on external surface
Γ_{int}	Boundary on internal surface
Γ_L	Boundary on top surface
Δr	Segment size of radial discretization, m
Δt	Time step, s
Δz	Segment size of axial discretization, m
λ	Thermal conductivity, W/m.K
σ_{meas}	Standard deviation for the measurement errors, K
σ_{model}	Standard deviation for the model errors, K
σ_{rw}	Standard deviation for the random walk parameter, W/m^2
Ω	Domain

amounts of heat to maintain some equipment's temperature within a desired range of operation and guarantee their proper working condition. In this sense, Pulsating Heat Pipes (PHPs) are an excellent choice for heating removal systems. Such cooling equipment operates as passive two-phase heat transfer devices, characterized by the oscillatory movement of the working fluid, providing high heat transfer capacity [1]. Also, their working principles allow their use in the absence of gravity, being of great interest for aerospace engineering applications [2].

Despite the fact that PHPs have been shown as a great option to solve some thermal issues in critical applications, their working principles are chaotic and complicated, and it is common to analyze PHPs' global performance through an equivalent thermal resistance [3,4]. From this point of view, the thermal performance of PHPs has a strong relation between the operation condition and the two-phase fluid-flow regime inside the PHP tubes [5]. Recent works provided some advances regarding the fluid behavior to characterize the PHP operation condition relating the local heat transfer between the working fluid and the PHP inner wall [6]. Some works, in fact, proposed the estimation of local heat fluxes on the inner surface of PHPs using non-intrusive techniques, through the solution of Inverse Heat Conduction Problems (IHCPs), with temperature measurements taken on the external wall by an infrared camera. Cattani et al. [7] proposed the thermal assessment of the wall-to-fluid heat flux along the adiabatic section of a Single Loop PHP (SLPHP), made of Sapphire and charged with Ethanol, based on the solution of a two-dimensional IHCP. In their work they used a high-speed and high-resolution infrared camera for temperature acquisition on the external pipe wall, showing that the proposed technique could provide means to infer the two-phase fluid-flow regime, based on the estimated heat flux. Pagliarini et al. [8] proposed a statistical approach to evaluate the wall-to-fluid heat flux along the adiabatic section of a multi-turn PHP made of Aluminum. An infrared camera measured the temperature on the external pipe wall over all channels. They solved an IHCP by filtering the measured temperature with a Gaussian filter and using a lumped one-dimensional heat conduction model for the inverse analysis. The results provided essential information about the fluid flow regimes and the oscillatory fluid behavior inside the tubes. Colaço et al. [9] applied the Conjugated Gradient Method (CGM) with Adjoint Operator to solve the IHCP based on the previous references [7] and [8]. The results were accurate when compared to the techniques used in the preceding works, with the advantage of less computational time and required memory. Pagliarini et al. [10] investigated a PHP heat transfer behavior regarding its heat load, orientation, and condenser temperature. A Gaussian filter allowed the local heat flux assessment along the adiabatic section, providing more insights into the PHP operation conditions. Iwata et al. [11] proposed an investigation of the thermal behavior of a micro-PHP with seven turns, and 46 % filled with HFC-134, by solving an IHCP with the Gaussian filter, and considering temperature measurements taken along the condenser section. Although these studies allowed a more detailed analysis of the working principles of PHPs, the proposed methodologies did not use real-time measurements in their analysis, but rather were applied to an offline estimation. Real-time estimation could be interesting to identify the operating condition of the PHP, as well to provide information about their thermal behavior during their functioning, especially under critical operational conditions before the system crisis (i.e., sudden increase of the device's thermal resistance or possibly a dry-out regime). Autonomous space travel missions, for example, where PHPs can be used to cool down electronic systems under low gravity conditions, could implement the proposed technique to acquire vital information about the internal heat flux, allowing the assessment of its functioning condition, and reducing the power consumption or shutting down the device being cooled down if the heat flux reaches a limit condition to avoid the complete system failure, resuming the operation after a period to continue the mission. Also, this powerful real-time monitoring would enable extending the operating range of these devices. Currently, large safety coefficients are used in the design phase of PHP to prevent undesirable device overheating, but these coefficients can be strongly reduced by developing original thermal control systems based on real-time monitoring.

For online control purposes, a software-based system named "soft sensors" is frequently used to achieve online control in the industry due to their reliability, low cost, and use for quality control, where measurement fusion obtains unobservable quantities under a system operation, possibly evaluated with KF [12]. The KF is a powerful control technique that is accurate and has low computational cost due to the sequential estimation of the states (i.e., temperature field, boundary conditions, and heat source) when new measurements are available, meaning that the data does not need to be stored as in the case of whole-

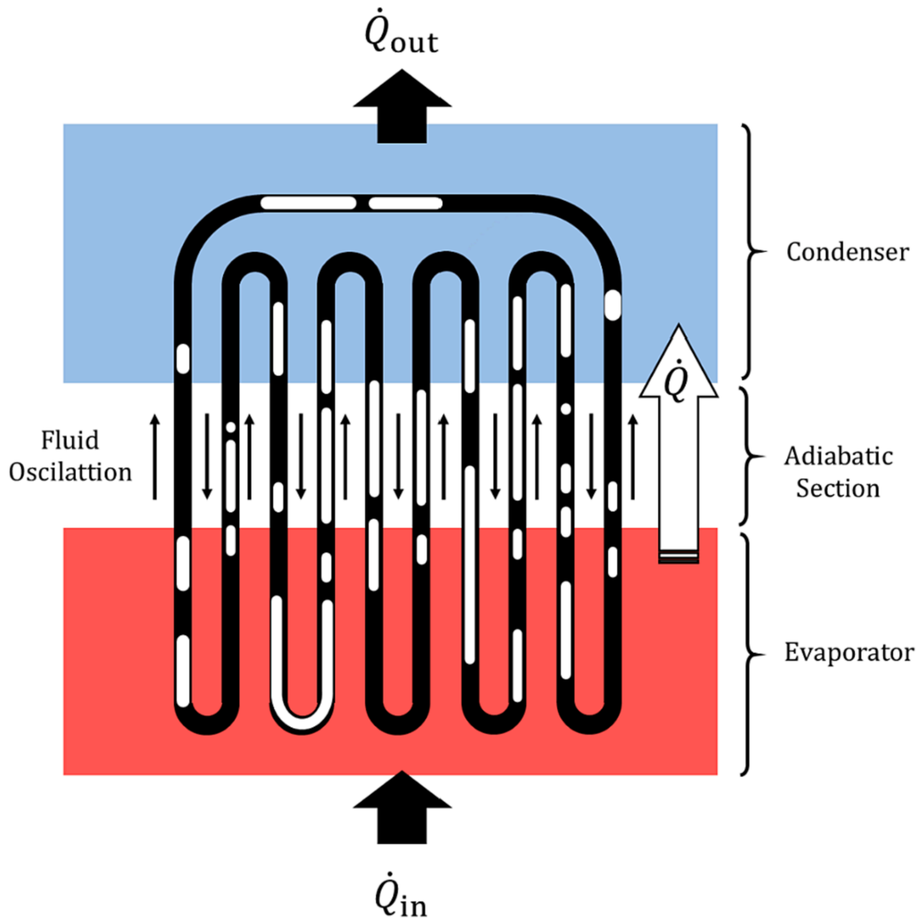

Fig. 1. Working principle of a PHP (Adapted from [2]).

domain inverse problem techniques [13]. When the problem is linear and has Gaussian noises, the KF provides the optimal estimation [14,15]. A large number of works concerning heat flux estimation using the KF for parameter estimation through the solution of IHCPs can be found in the literature. Ji et al. [16] proposed the solution of an IHCP with an online estimation algorithm based on the KF and the Recursive Least-Squares Estimation (RLSE) for a one-dimensional heat conduction problem. The authors obtained the estimation of a time-varying heat flux in one side of the domain considering available temperature measurement on the opposite surface. Tuan et al. [17] extended the previous work to a two-dimensional heat conduction problem. The authors used the KF-RLSE for the heat flux online estimation in a heat conduction problem, obtaining satisfactory results. Tuan et al. [18] used the KF-RLSE estimation methodology for an online heat flux time-varying estimation in a two-dimensional heat conduction problem, presenting accurate results. Later, Tuan et al. [19] performed a heat flux estimation with the KF-RLSE, considering a one-dimensional heat conduction problem in radial coordinates, showing the potential of the estimation methodology. Also, Noh *et al.* [20] showed an application of the KF-RLSE to evaluate the heat flux on gun barrels in a complex three-dimensional geometry by solving an inverse heat conduction problem. Additionally, many works studied the methodology performance considering different boundary conditions to evaluate the estimation performance of KF [21–26].

Regarding the parameter estimation approach, Daouas et al. [27] proposed the heat flux estimation with the augmented state vector technique, which models the parameters as states to be estimated. The study used the Extended Kalman Filter to solve a nonlinear IHCP to obtain the heat flux estimation. Orlande et al. [28] proposed using the KF to assess the heat flux by adopting the augmented state vector technique considering a lumped heat conduction model, providing a good estimation for the heat flux. Pacheco et al. [29] used the KF to estimate the high-magnitude heat flux position using an improved lumped model. The augmented state vector technique presents the advantage of performing only one calculation stage instead of two from the previous approaches [30], and it was the strategy adopted in this paper.

Thus, since the previously listed works showed good performance on online heat flux estimation using the KF to solve the IHCP, the current work evaluates the KF capability for heat flux estimation along PHPs adiabatic section. Since the proposed problem is linear and (ideally) subjected to a Gaussian noise, the KF provides the optimal solution methodology. For the inverse problem, the temperature measurements are available on the external surface of the tube, obtained via an infrared camera. The advantages of the proposed application are its non-intrusive character, the simplicity for computational implementation, and the low computational time and memory required, therefore applicable for real-time applications, possibly on some embarked devices. The results were verified against other technique for synthetic data and validated for real experimental measurements.

It is worth mentioning that other techniques, not based on inverse problems, could be used for estimating the internal heat flux, but would suffer from other problems. For instance, regarding the possibility of obtaining similar results with conventional methods, such as using an array of thermocouples and not filtering the measured temperatures, several challenges emerge. The foremost and most significant issue relates to the ill-posed nature of the inverse heat conduction problem. This nature implies sensitivity to fluctuations in input data caused by experimental noise, making direct calculation of the Laplacian of raw data, as per Eq. (1a) to be presented further, unfeasible due to noise

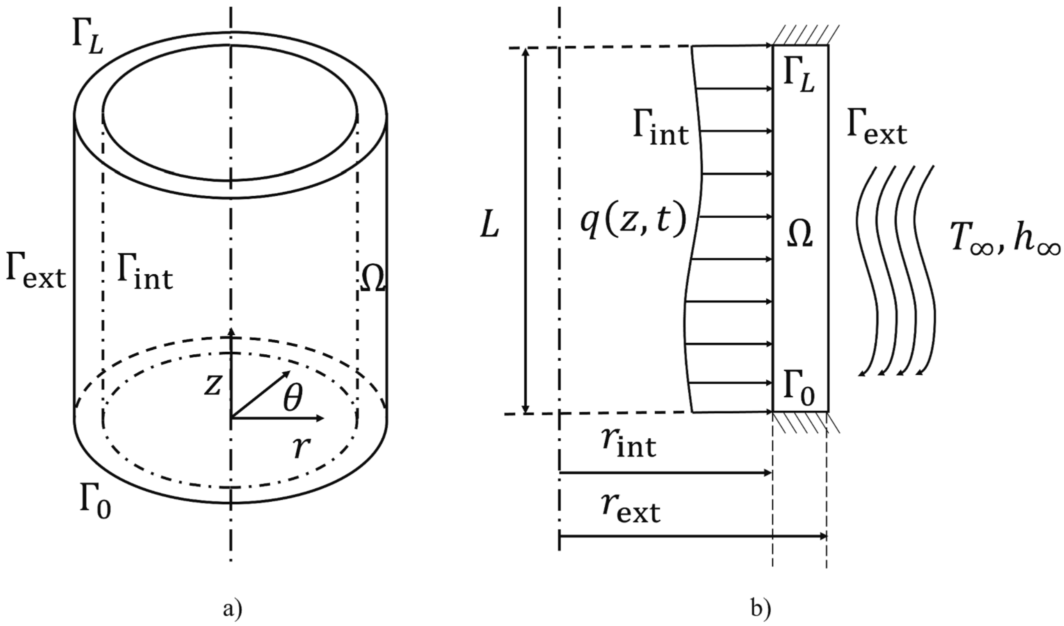

Fig. 2. Physical domain for the Pulsating Heat Pipe (a) and pipe wall domain (b).

interference. Indeed, the nth derivative is a linear operator that functions as a filtering operator, amplifying the high-frequency components of a given set of input data more than the low-frequency ones. In nearly all practical situations related to heat transfer, the frequency components of the exact signal tend to concentrate in the low spatial frequency range of the spectrum. Meanwhile, noise, typically Gaussian, is uniformly distributed in the spatial frequency domain. The proposed solution strategy, based on the KF, addresses this issue by treating the raw input temperature data to reconstruct the second derivative of the signal. The second issue preventing similar results with conventional methods, like an array of thermocouples, is associated with the wall temperature's temporal and spatial variations due to the fast oscillations of the two-phase flow inside the PHP. Such variations are challenging for thermocouples to accurately detect, considering problems related to sensor sensitivity, time constants, and the need for a high number of sensors for proper spatial distribution of the heat flux. Therefore, we believe the proposed technique would help experimentalists to estimate internal heat fluxes in PHPs and possibly inferring the two-phase fluid-flow regimes inside these devices.

2. Direct model

PHPs work partially filled with a fluid that transfers heat from a hot heat source to a cold one. The hot source warms the pipe wall and transfers heat to the working fluid. A phase change occurs within the working fluid, creating a two-phase flow with higher temperature and pressure, which therefore acts like a pump, pushing the fluid to release heat to the colder section, named condenser [2]. Generally, the section between these two zones is known as the adiabatic section, which transfers low heat quantity. The fluid cools down and condensates in the colder part of the PHP and returns back to the evaporator, repeating the cycle. Fig. 1 presents a schematic of PHP operation.

In this work, only the solid PHP wall is analyzed. The direct problem consists of modeling it as a heat conduction problem. Such model simulates the heat exchange between the fluid and the pipe wall and was used to solve the inverse problem. The direct problem considers a hollow cylinder, shown in Fig. 2a, defined by a domain Ω representing the adiabatic section of a PHP device. The easy accessibility for temperature measurements be taken by an infrared camera in the adiabatic zone (during the inverse problem part of this work) justifies its choice to be used as a modelling region for the direct problem. The material properties of the pipe wall such as thermal conductivity, λ, specific heat at constant pressure, c_p, and density, ρ, are considered constant. To emulate the actual PHP working conditions, it is considered that the pipe's inner surface, Γ_{int}, is subjected to a prescribed time and space-varying heat flux $q(z,t)$, representing the heat exchanged between the solid wall and the working fluid in the PHP during its operation. The internal heat flux might assume positive or negative values depending on the direction of the fluid flow. On the opposite side, the outer surface, Γ_{ext}, exchanges heat by convection with the environment with temperature T_∞ and convective heat transfer coefficient h_∞. The other two surfaces, Γ_0 and Γ_L, are considered thermally insulated. The tube length is L, and the inner and outer radius are defined by r_{int} and r_{ext}, respectively. The above-described boundary conditions are consistent with what has been experimentally observed and verified in previous works [7,8], and are depicted in Fig. 2.b.

Due to experimental observation from [7,8] the temperature variation over the angular direction can be neglected and the heat conduction equation becomes a two-dimensional problem in r and z, as shown in Eqs. (1.a)–(1.f).

$$\frac{1}{\alpha}\frac{\partial T}{\partial t} = \frac{1}{r}\frac{\partial T}{\partial r} + \frac{\partial^2 T}{\partial r^2} + \frac{\partial^2 T}{\partial z^2} \quad \text{in} \quad \Omega \tag{1.a}$$

$$-\lambda \left.\frac{\partial T}{\partial r}\right|_{r=r_{int}} = q(z,t) \quad \text{on} \quad \Gamma_{int} \tag{1.b}$$

$$-\lambda \left.\frac{\partial T}{\partial r}\right|_{r=r_{ext}} = h_\infty (T - T_\infty) \quad \text{on} \quad \Gamma_{ext} \tag{1.c}$$

$$\left.\frac{\partial T}{\partial z}\right|_{z=0} = 0 \quad \text{on} \quad \Gamma_0 \tag{1.d}$$

$$\left.\frac{\partial T}{\partial z}\right|_{z=L} = 0 \quad \text{on} \quad \Gamma_L \tag{1.e}$$

$$T(r,z,t=0) = T_0(r,z) \quad \text{in} \quad \Omega \quad \text{for} \quad t = 0 \tag{1.f}$$

where α is the thermal diffusivity of the material. The solution for the forward problem is achieved by using the Finite Difference Method [31].

3. Inverse problem

The inverse problem considered in this work concerns the internal heat flux estimate on PHPs assuming that temperature measurements are available on the pipe's external surface. The problem under question is also defined as a nonstationary inverse problem [15] since the physical quantities involved in the problem are time dependent. We can proceed with the inverse problem solution by considering the state estimation approach, where the main goal is to obtain information about desired quantities by correlating them with the available measurements. Firstly, we consider the evolution in time of the state vector, $\mathbf{x}_k \in \mathbb{R}^{nx}$, where n_x is the dimension of the state vector, described by the discrete-time stochastic model:

$$\mathbf{x}_{k+1} = \mathbf{f}_k(\mathbf{x}_k, \mathbf{u}_k, \mathbf{v}_k) \tag{2}$$

where k and $k+1$ stand for the k^{th} and $(k+1)^{\text{th}}$ time instant, respectively, the vector $\mathbf{x}_k$ contains all desired states to be estimated (temperatures and heat fluxes in the context of this paper), $\mathbf{u}_k$ is the input (or control) vector, $\mathbf{v}_k$ is the process noise sequence, and $\mathbf{f}_k(\cdot)$ is a known function (possibly non-linear) that describes the evolution of the states over time. The main goal of the state estimation problem is to obtain $\mathbf{x}_{k+1}$ considering that measurements $\mathbf{z}_{k+1} \in \mathbb{R}^{nz}$ are available. The observation model is therefore defined as:

$$\mathbf{z}_{k+1} = \mathbf{h}_{k+1}(\mathbf{x}_{k+1}, \mathbf{w}_{k+1}) \tag{3}$$

where $\mathbf{h}(\cdot)$ is a known function, possibly non-linear, and $\mathbf{w}_{k+1}$ is the measurement noise. This function returns all the measurable states from vector $\mathbf{x}_{k+1}$. When the pair *evolution-observation* models are linear and Gaussian, the KF statistically provides the optimal estimation [14]. In this sense, Eqs. (2) and (3) are rewritten as:

$$\mathbf{x}_{k+1} = \mathbf{F}_k\mathbf{x}_k + \mathbf{u}_k + \mathbf{v}_k \tag{4}$$

$$\mathbf{z}_{k+1} = \mathbf{H}_{k+1}\mathbf{x}_{k+1} + \mathbf{w}_{k+1} \tag{5}$$

where $\mathbf{F}_k$ and $\mathbf{H}_{k+1}$ are the evolution and observation matrices, respectively. In this work, the estimation problem is defined as a filtering problem due to the online control purpose [14,15], which consists of two basic steps: prediction and update. The evolution model forecasts the states from instant k to the next instant $k+1$, considering available known prior information. When new measurements are available, represented by the observation model, the predicted states are corrected during the update step according to Bayes' theorem [14,15]. Consequently, a new prediction step is performed with the corrected state until new measurements are available to correct the predicted states. This procedure is repeated sequentially until the final time of the experiment.

In the current work, the matrices $\mathbf{F}_k$ and $\mathbf{H}_{k+1}$ and the input vector $\mathbf{u}_k$ from Eqs. (4) and (5) do not change over time and, consequently, the subscripts k and $k+1$ of these matrices are omitted. Therefore, considering $\mathbf{P}_k$ the covariance of the state vector concerning the instant k, $\mathbf{Q}_k$ and $\mathbf{R}_{k+1}$ the covariance matrices related to the process, and measurement noises $\mathbf{v}_k$ and $\mathbf{w}_{k+1}$, the KF equations for prediction and update steps are defined by Eqs. (6.a) and (6.b) and (7.a)–(7.c), respectively [14,15].

Prediction:

$$\widehat{\mathbf{x}}_{k+1|k} = \mathbf{F}\widehat{\mathbf{x}}_{k|k} + \mathbf{u} \tag{6.a}$$

$$\mathbf{P}_{k+1|k} = \mathbf{F}\mathbf{P}_{k|k}\mathbf{F}^{\mathrm{T}} + \mathbf{Q}_k \tag{6.b}$$

Update:

$$\mathbf{K}_{k+1} = \mathbf{P}_{k+1|k}\mathbf{H}^{\mathrm{T}}\left(\mathbf{H}\mathbf{P}_{k+1|k}\mathbf{H}^{\mathrm{T}} + \mathbf{R}\right)^{-1} \tag{7.a}$$

$$\widehat{\mathbf{x}}_{k+1|k+1} = \widehat{\mathbf{x}}_{k+1|k} + \mathbf{K}_{k+1}\left(\mathbf{z}_{k+1} - \mathbf{H}\widehat{\mathbf{x}}_{k+1|k}\right) \tag{7.b}$$

$$\mathbf{P}_{k+1|k+1} = (\mathbf{I} - \mathbf{K}_{k+1}\mathbf{H})\mathbf{P}_{k+1|k} \tag{7.c}$$

The hat "^" over the state vector means the estimate of the vector state. Notice that the subscript related to time instant in matrices **F**, **u** and **R** is omitted since they do not vary in time, and $\mathbf{K}_{k+1}$ is defined as the Kalman Gain matrix. The superscript "T" denotes the transpose, the subscript k and $k+1$ are the priori and posteriori time instant, respectively, of the vector or matrix, the subscript "$k+1|k$" means the prediction, and "$k|k$" and "$k+1|k+1$" represent the corrected states at k and $k+1$ time instant.

In brief words, the state vector $\mathbf{x}_{k+1|k}$ and the covariance model matrix $\mathbf{P}^{-}_{k+1}$ are predicted for the future time using the prior information and the evolution model in the prediction step. When the measurements are available, the states and the covariance model matrix are corrected by the Kalman Gain matrix during the update step. Thus, the corrected state $\mathbf{x}_{k+1|k+1}$ and covariance matrix $\mathbf{P}_{k+1}$ are the initial condition for the next time step. Thus, the procedures of prediction and update are repeated recursively over the time until the end of the experiment.

The augmented state technique is then employed to estimate the temperature and heat fluxes [27]. In this case, we define the target state vector to be estimated by:

$$\mathbf{x}_k^{\text{aug}} = \begin{bmatrix} \mathbf{T}_k \\ \mathbf{q}_k \end{bmatrix} \tag{8}$$

where $\mathbf{T}_k = \left[T_k^1, T_k^2, \cdots, T_k^{N_z-1}, T_k^{N_z}, T_k^{N_z+1}, \cdots, T_k^{2N_z}, \cdots, T_k^{N_r\times N_z-1}, T_k^{N_r\times N_z}\right]^{\mathrm{T}}$ are the estimated temperature of the nodes and $\mathbf{q}_k = \left[q_k^1, q_k^2, \cdots, q_k^{N_z-1}, q_k^{N_z}\right]^{\mathrm{T}}$ are the estimated heat flux of the nodes on the wall, N_r and N_z are the total number of estimation nodes on the radial and axial coordinates, respectively. In this approach, the parameter estimation is performed by considering the heat flux as a state variable.

The evolution over time for the temperature is achieved by using the Finite Difference Method with the explicit scheme [31]. On the other hand, since the heat flux evolution over time is unknown, it was modelled by a black-box random walk model [27], which is defined by Eq. (9), where $\boldsymbol{\xi}$ is a Gaussian random sequence with zero mean and unity standard deviation, and σ_{rw} is the step-size.

$$\mathbf{q}_{k+1} = \mathbf{q}_k + \boldsymbol{\xi}\sigma_{\text{rw}} \tag{9}$$

Hence, considering the Finite Difference Method with the explicit scheme as the evolution model for the temperature, we can write the matrices and vectors of the KF according to the following equations:

$$\mathbf{F} = \begin{bmatrix} \mathbf{F}_{\mathbf{fdm}\,N_rN_z\times N_rN_z} & \begin{matrix} \dfrac{2\delta r}{\lambda}\left(-\dfrac{\alpha\delta t}{2r_{\text{int}}\delta r} + r_r\right)\mathbf{I}_{N_z\times N_z} \\ \mathbf{0}_{(N_zN_r-N_z)\times N_z} \end{matrix} \\ \mathbf{0}_{N_z\times N_rN_z} & \mathbf{I}_{N_z\times N_z} \end{bmatrix} \tag{10.a}$$

$$\mathbf{H} = \begin{bmatrix} \mathbf{0}_{N_z\times(N_rN_z-N_z)} & \mathbf{I}_{N_z\times N_z} & \mathbf{0}_{N_z\times N_z} \end{bmatrix} \tag{10.b}$$

$$\mathbf{Q}_k = \begin{bmatrix} \sigma^2_{\text{model}}\mathbf{I}_{N_r\times N_z} & \mathbf{0}_{N_z\times N_z} \\ \mathbf{0}_{N_r\times N_z} & \sigma^2_{\text{rw}}\mathbf{I}_{N_z\times N_z} \end{bmatrix} \tag{10.c}$$

$$\mathbf{R} = \left[\sigma_{\text{meas}}\mathbf{I}_{N_z\times N_z}\right] \tag{10.d}$$

$$\mathbf{u} = \begin{bmatrix} \mathbf{0}_{N_rN_z-N_z\times 1} \\ \dfrac{2T_\infty h_\infty \delta r}{\lambda}\left(\dfrac{\alpha\delta t}{2r_{\text{ext}}\delta r} + r_r\right)\mathbf{I}_{N_z\times 1} \end{bmatrix} \tag{10.e}$$

The matrix $\mathbf{F}_{\text{fdm}}$ is obtained by the finite-difference discretization of the 2D heat conduction model. The representation of this matrix can be complex and consequently we present a pseudo-code to build it in Appendix I, where the matrix $\mathbf{F}_{\text{fdm}}$ is considered initially a zero matrix with dimension of $N_rN_z \times N_rN_z$. The matrix $\mathbf{I}_{axb}$ represents an identity matrix

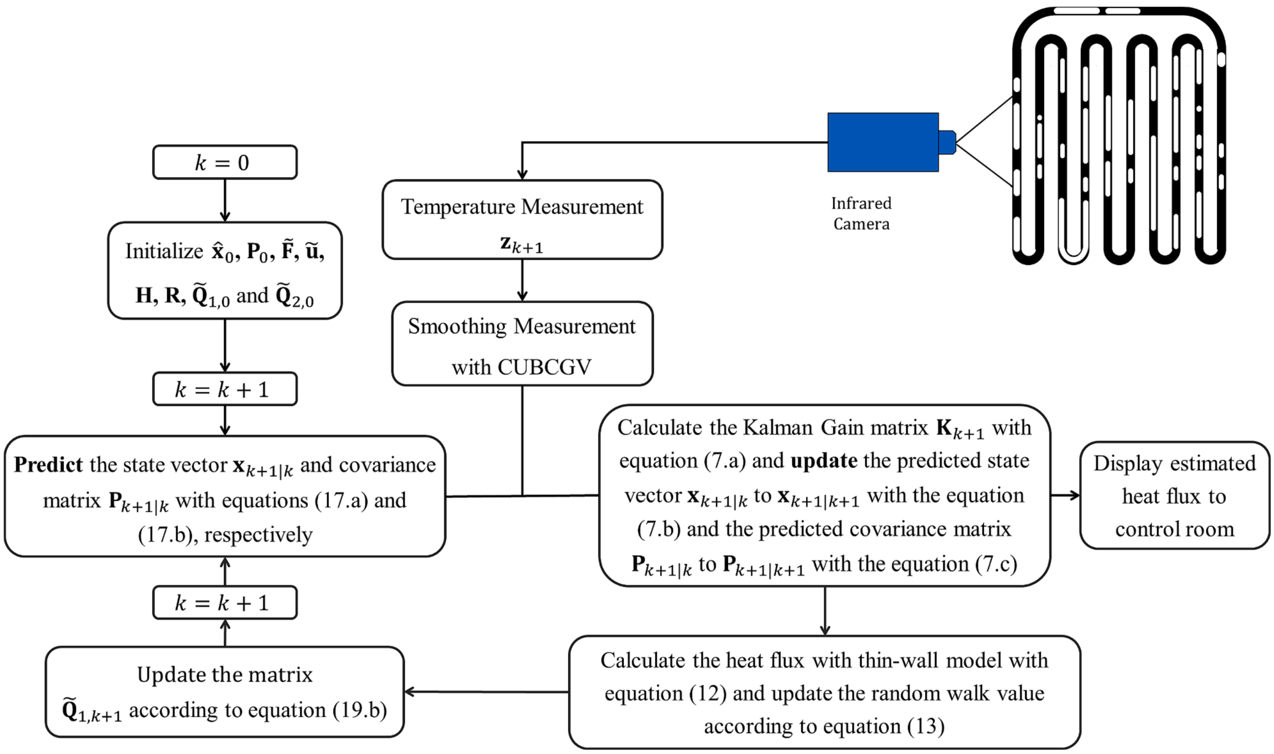

Fig. 3. Flowchart presenting the recursive estimation with Kalman filter with prediction step optimized.

of size a by b.

3.1. Random walk parameter control

The parameter σ_{rw} influences the evolution model of the estimated heat flux. Its tuning can be difficult and problem dependent, meaning that one particular value could work well for a specific problem but not for another one. In order to optimize such tuning, we propose a methodology for calculating σ_{rw} for each time step. Therefore, in order to perform an automatic correction of σ_{rw} on each measurement time step, a one-dimensional lumped model of the system is considered in the same form as in reference [8], represented by the following equations:

$$\frac{1}{\alpha}\frac{\partial T}{\partial t} = \frac{\partial^2 T}{\partial z^2} + C_1 q(z,t) + C_2 T + C_3 \text{ in } \Omega \tag{11.a}$$

$$\left.\frac{\partial T}{\partial z}\right|_{z=0} = 0 \text{ on } \Gamma_0 \tag{11.b}$$

$$\left.\frac{\partial T}{\partial z}\right|_{z=L} = 0 \text{ on } \Gamma_L \tag{11.c}$$

$$T(z, t=0) = T_0(z) \text{ in } \Omega \text{ for } t = 0 \tag{11.d}$$

where:

$$C_1 = \frac{2r_{\text{int}}}{\lambda\left(r_{\text{ext}}^2 - r_{\text{int}}^2\right)} \tag{11.e}$$

$$C_2 = -\frac{2r_{\text{int}}h_\infty}{\lambda\left(r_{\text{ext}}^2 - r_{\text{int}}^2\right)} \tag{11.f}$$

$$C_3 = \frac{2r_{\text{int}}h_\infty T_\infty}{\lambda\left(r_{\text{ext}}^2 - r_{\text{int}}^2\right)} \tag{11.g}$$

By using the Finite Difference Method [31] in Eq. (11.a), for the lumped model, and rearranging the terms, we can obtain the heat flux as:

$$q_k^{i,\text{model}} = \frac{\frac{1}{\alpha}\left(\frac{\widehat{T}_{k+1}^{i} - \widehat{T}_k^{i}}{\Delta t_{\text{meas}}}\right) - \frac{\widehat{T}_k^{i+1} - 2\widehat{T}_k^{i} + \widehat{T}_k^{i-1}}{\Delta z^2} - C_2\widehat{T}_k^i - C_3}{C_1} \tag{12}$$

where the temperature $\widehat{T}_k^i$ is the filtered temperature at node i in the time instant k obtained by KF and δt_{meas} and δz are the measurement time step and space discretization, respectively. We can therefore correct the parameter σ_{rw} by setting:

$$\sigma_{rw}' = \frac{\sum_{i=1}^{N_{\text{nodes}}} q_k^{i,\text{est}} - q_k^{i,\text{model}}}{N_{\text{nodes}}} \tag{13}$$

where $q_k^{i,\text{est}}$ is the estimated heat flux by KF and $q_k^{i,\text{model}}$ is the heat flux resulting from the lumped model. In this way, instead of selecting a constant random walk parameter σ_{rw}, its value can be computed at the new time step according to Eq. (13) and replaced on the covariance matrix of states $\mathbf{Q}_k$ in Eq. (10.c) to be used in the next prediction step.

3.2. Rearrangement of the prediction matrices to guarantee the stability condition of the Finite Difference Method

As mentioned in the description of the direct problem, the explicit finite-difference scheme needs to comply with the Courant-Friedrichs-Lewy condition to guarantee the stability of the solution [31]. In this work, the time step considered for the direct problem solution is smaller than the time between measurements, which means that the prediction step needs to compute the evolution of the states N_t times until the measurements are available. Specifically, N_t is calculated as the required number of time steps of the finite difference method, with Δt respecting the stability condition, to reach the time step of measurements, Δt_{meas}, i.e. N_t is the ratio between Δt_{meas} and Δt. However, this procedure consumes a lot of computational time. Therefore, knowing that the matrices $\mathbf{F}$ (as well its transpose) and $\mathbf{Q}_k$, as well as the input vector $\mathbf{u}$, are time invariant between the measurements, the calculation of the prediction step can be optimized by performing the following procedure. The

Table 1
Parameters considered for the case with synthetic data.

Property/Geometry	Aluminum Tube [8]
L[m]	0.1
$t_{\text{experiment}}$[s]	20
r_{int}[m]	0.0015
r_{ext}[m]	0.0025
λ[W/m.K]	201
ρ[kg/m^3]	2700
c_p[J/kg.K]	900
T_∞[K]	295.15
h_∞[W/m^2.K]	10
Δz_{meas}[m]	0.001
Δt_{meas}[s]	0.02
N_r	6
N_z	101
N_{time}	1001

Table 2
Average RMS errors between exact and estimated heat fluxes for the synthetic data with KF and CGM with AO [9].

A[W/m^2]	p[Hz]	Method	Average RMS Error E_q[%]		
			σ_{meas} = 0.01K	σ_{meas} = 0.06K	σ_{meas} = 0.1K
2000	0.6	KF	10.74	25.54	31.66
		CGM with AO [9]	3.06	5.74	7.66
	0.8	KF	12.80	32.77	34.96
		CGM with AO [9]	3.20	6.80	9.64
	1.0	KF	19.19	34.70	33.79
		CGM with AO [9]	3.33	8.33	12.74
	1.2	KF	21.4	34.01	31.05
		CGM with AO [9]	3.53	10.37	16.65
4000	0.6	KF	12.83	18.65	21.96
		CGM with AO [9]	5.03	8.77	10.68
	0.8	KF	14.14	22.69	31.23
		CGM with AO [9]	5.07	9.17	12.20
	1.0	KF	15.43	29.30	35.04
		CGM with AO [9]	5.25	10.49	14.73
	1.2	KF	16.79	35.91	35.27
		CGM with AO [9]	5.54	12.29	17.63

procedure considers the prediction of the state vector from the priori at time k, $\widehat{\mathbf{x}}_k$, to time when the measurement is available $k+N_t$, giving $\mathbf{x}_{k+N_t|k}$, where the evolution vector is calculated with respect to the time step Δt from finite differences method. Therefore, we obtain:

$$\widehat{\mathbf{x}}_{k+1|k} = \mathbf{F}\widehat{\mathbf{x}}_{k|k} + \mathbf{u} \tag{14}$$

Now, if we repeat the process $k+N_t$ times, we obtain:

$$\widehat{\mathbf{x}}_{k+N_t|k} = \widetilde{\mathbf{F}}\mathbf{x}_{k|k} + \sum_{i=0}^{N_t-1}(\mathbf{F})^i\mathbf{u} = \widetilde{\mathbf{F}}\widehat{\mathbf{x}}_{k|k} + \widetilde{\mathbf{u}} \tag{15}$$

where $\widetilde{\mathbf{F}} = (\mathbf{F})^{N_t}$ and $\widetilde{\mathbf{u}} = \sum_{i=0}^{N_t-1}(\mathbf{F})^i\mathbf{u}$. The notation $(\mathbf{F})^a$ means that the matrix $\mathbf{F}$ is multiplied a times by itself. It should be noticed that this procedure can be followed since the matrix $\mathbf{F}$ and $\mathbf{u}$ are invariant over time.

Now, similarly as outlined above, the covariance matrix for times $k + N_t$ can be obtained as:

$$\mathbf{P}_{k+N_t|k} = \widetilde{\mathbf{F}}\mathbf{P}_{k|k}\widetilde{\mathbf{F}}' + \widetilde{\mathbf{Q}}_k \tag{16}$$

where $\widetilde{\mathbf{F}}' = \left(\mathbf{F}^{\mathrm{T}}\right)^{N_t}$ and $\widetilde{\mathbf{Q}}_k = \sum_{i=0}^{N_t-1}(\mathbf{F})^i\mathbf{Q}_k\left(\mathbf{F}^{\mathrm{T}}\right)^i$. Therefore, we can rewrite the prediction step by replacing Eqs. (15) and (16), resulted from the previous procedure, in Eqs. (6.a) and (6.b). Notice that the subscript $k+N_t$ is replaced by $k+1$ to define the next time step when the measurement is available.

$$\widehat{\mathbf{x}}_{k+1|k} = \widetilde{\mathbf{F}}\widehat{\mathbf{x}}_{k|k} + \widetilde{\mathbf{u}}_k \tag{17.a}$$

$$\mathbf{P}_{k+1|k} = \widetilde{\mathbf{F}}\mathbf{P}_{k|k}\widetilde{\mathbf{F}}' + \widetilde{\mathbf{Q}}_k \tag{17.b}$$

The correction of the parameter σ_{rw} requires a new approach for matrix $\widetilde{\mathbf{Q}}_k$. We can rewrite this matrix in the following form:

$$\widetilde{\mathbf{Q}}_k = \sum_{i=0}^{N_t-1}(\mathbf{F})^i\mathbf{Q}_k\left(\mathbf{F}^{\mathrm{T}}\right)^i = \sum_{i=0}^{N_t-1}(\mathbf{F})^i\begin{bmatrix}\sigma^2_{\text{model}}\mathbf{I}_{N_r\times N_z} & \mathbf{0}_{N_z\times N_z}\\ \mathbf{0}_{N_r\times N_z} & \sigma^2_{\text{rw}}\mathbf{I}_{N_z\times N_z}\end{bmatrix}\left(\mathbf{F}^{\mathrm{T}}\right)^i \tag{18}$$

Hence, by splitting the process into two identity matrices, and considering that σ^2_{model} and σ'^2_{rw} are constants for each time interval between measurements, we obtain:

$$\widetilde{\mathbf{Q}}_k = \widetilde{\mathbf{Q}}_{1,k} + \widetilde{\mathbf{Q}}_{2,k} \tag{19.a}$$

where:

$$\widetilde{\mathbf{Q}}_{1,k} = \sigma^2_{\text{model}}\left\{\sum_{i=0}^{N_{\text{model}}-1}(\mathbf{F})^i\left(\begin{bmatrix}\mathbf{I}_{N_r\times N_z} & \mathbf{0}_{N_z\times N_z}\\ \mathbf{0}_{N_r\times N_z} & \mathbf{0}_{N_z\times N_z}\end{bmatrix}\right)\left(\mathbf{F}^{\mathrm{T}}\right)^i\right\} \tag{19.b}$$

$$\widetilde{\mathbf{Q}}_{2,k} = \sigma'^2_{\text{rw}}\left\{\sum_{i=0}^{N_{\text{model}}-1}(\mathbf{F})^i\left(\begin{bmatrix}\mathbf{0}_{N_r\times N_z} & \mathbf{0}_{N_z\times N_z}\\ \mathbf{0}_{N_r\times N_z} & \mathbf{I}_{N_z\times N_z}\end{bmatrix}\right)\left(\mathbf{F}^{\mathrm{T}}\right)^i\right\} \tag{19.c}$$

Noticing that the first term related to the modelling error is constant over the time, we can finally write the second term related to the random walk parameter as a single multiplication as presented in Eq. (13). In this case, Eq. (19.a) can be used by substituting it in Eq. (17.b),

The above description provides an essential advantage to reduce the number of multiplication operations between matrices and vectors during the prediction step, i.e., instead of performing the multiplication N_t times on Eqs. (6.a) and (6.b) to reach the instant of temperature acquisition, we only perform it once. Hence, Fig. 3 presents the proposed methodology to estimate the internal heat flux with the KF approach, considering the optimized procedure for the prediction step.

4. Results and discussion

In the present work, the KF was applied for heat flux estimation based on the test cases taken from [8], which refers to a PHP made of aluminum, operating under microgravity conditions with a filling ratio of 50 %. The Gaussian Filter (GF) was adopted in [8] to estimate the internal heat flux on the PHP. Later, Colaço *et al.* [9] used the Conjugate Gradient Method with Adjoint Operator (CGM with AO) to this same test case [8], since the CGM with AO is an auto-regularization technique that does not depend on any tunning parameter. In both cases, the Morozov Principle [32] was used to stop the iterative procedures. Initially, synthetic data were considered, and then estimates with experimental data were conducted. The results with the KF for the heat flux estimation considering synthetic data are compared against the exact ones. For the experimental data, since the real value of the heat flux is not known, the results are compared with the ones obtained by the CGM with AO [9].

4.1. Synthetic data

The estimation procedure begins with the KF technique by considering synthetic data generated by a model built under the COMSOL® Multiphysics software, which alleviates the inverse crime since the method used for the synthetic data generation is different [33] from the

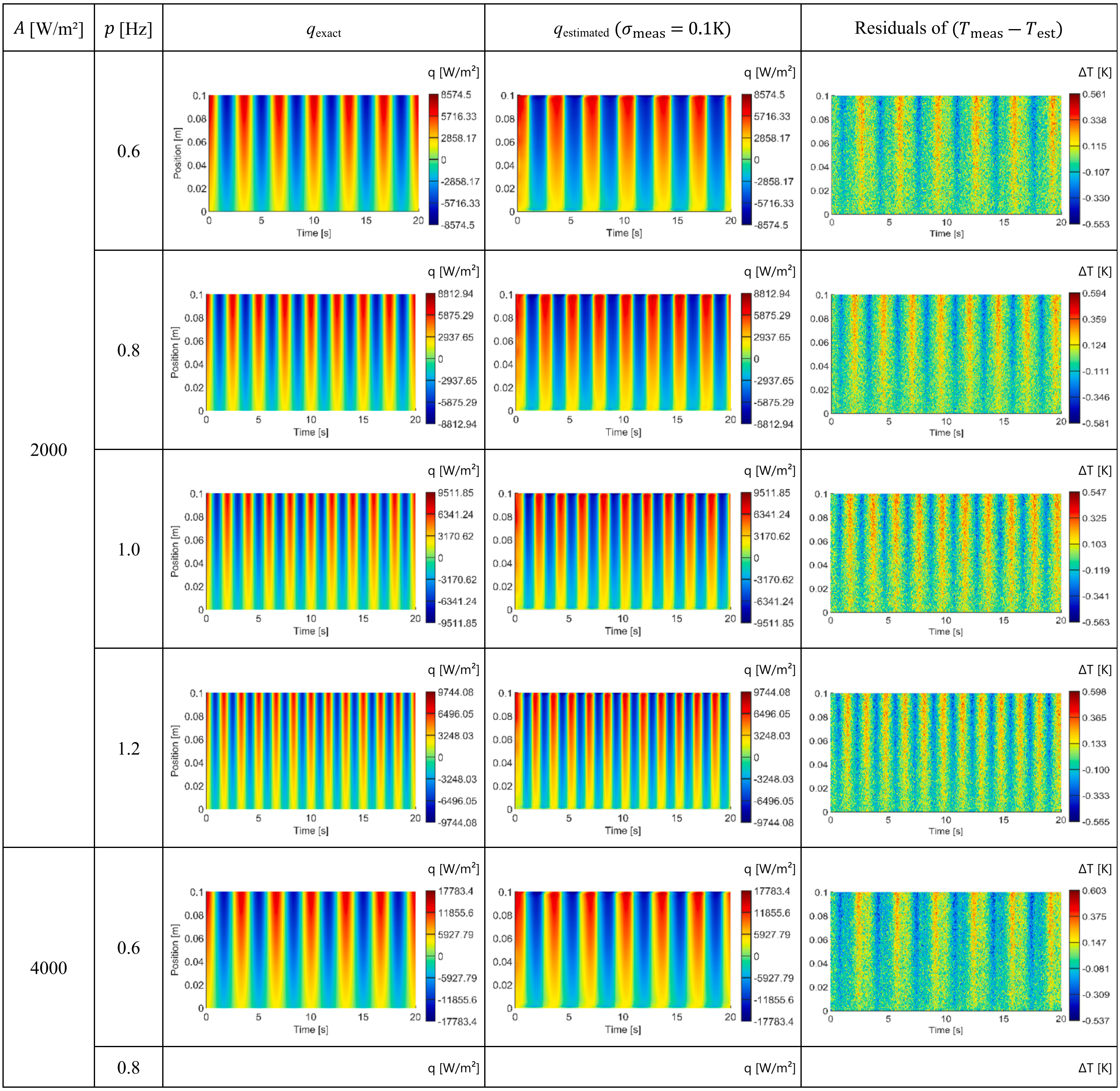

Fig. 4. Exact and estimated heat fluxes, and temperature residuals for the case with synthetic data.

one used in the inverse problem. The temperature is extracted on the external wall surface and random Gaussian noises are added to generate the synthetic measurement, as it is described in the following equation:

$$\mathbf{T}_{\text{meas}} = \mathbf{T}_{\text{exact}} + \boldsymbol{\varepsilon}\sigma_{\text{meas}} \tag{20}$$

where σ_{meas} represents the standard deviation of the measurements and $\boldsymbol{\varepsilon}$ is a white random Gaussian sequence with unity standard deviation. The parameters considered for solving the direct problem are presented in Table 1.

To generate the synthetic data, the exact heat flux function is considered to vary dynamically in time and space to reproduce the oscillatory behavior of the fluid flow inside the tube, as suggested by Colaço *et al.* [9]. In this sense, the heat flux is defined by the following equation:

$$q(z,t) = A\cos(\pi pt)\left[1+\left(\frac{z}{\Delta z}+1\right)\frac{L}{8}\right] \tag{21}$$

where A [W/m^2] represents the amplitude of the heat flux and p [Hz] represents the frequency of fluid flow oscillation along the adiabatic section. It should be noticed that the above equation provides positive and negative values of heat flux, where positive heat fluxes mean that hot vapor plugs and liquid slugs are moving from the evaporator to the condenser, while negative values represent a cold liquid flowing reversely from the condenser to the evaporator at a lower temperature than the channel wall previously heated [8]. To evaluate the average difference between the estimated and the exact heat fluxes we adopt the following equation for the RMS error:

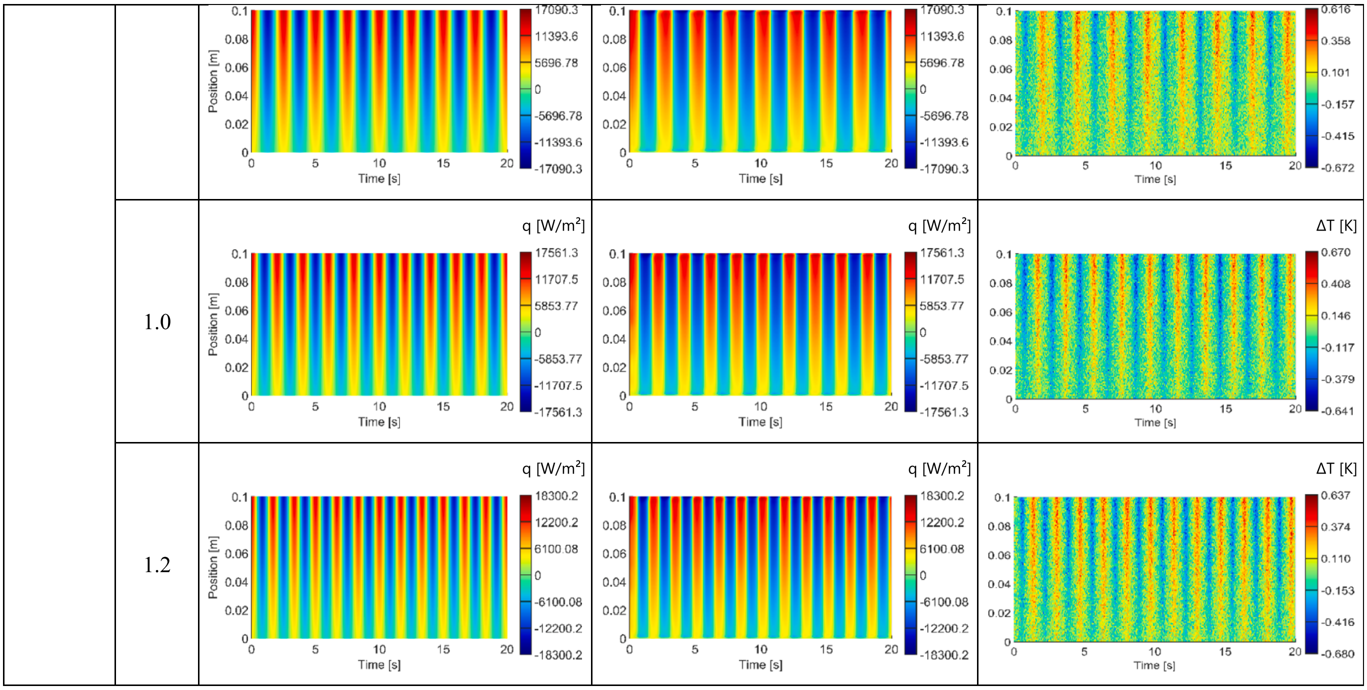

Fig. 4. (*continued*).

$$E_q = \frac{\|\boldsymbol{q}_{\text{estimated}} - \boldsymbol{q}_{\text{exact}}\|_2}{A\sqrt{N_{\text{space}}N_{\text{time}}}} \tag{22}$$

where N_{space} and N_{time} are the number of measurements in space and time, respectively. The computational code for the inverse problem was implemented in FORTRAN language. The CPU used for the simulations was an Apple Silicon M1 chip.

The mesh used to solve the inverse problem in this case is considered to have 6 nodes on radial direction (N_r) and 101 nodes on the axial direction (N_z). Three different measurement noise levels were considered to analyze the KF performance.

In order to regularize the measured temperatures to be used in the KF, a smoothing cubic spline with generalized cross-validation was applied over the space, for each measurements time step. The calculation routine used to smooth the temperature was the CUBGCV (Cubic Smoothing Spline with Generalized Cross-Validation) routine from [34].

The parameter A varied from 2000 to 4000 W/m^2, while p varied from 0.6 to 1.2 Hz. The results for the average RMS error with KF and CGM with AO [9] are presented in Table 2. The estimated heat flux with the KF provided a delayed response when compared to the exact one, resulting in high values of RMS error. Therefore, to allow a fair evaluation with the estimated heat flux with KF, the solution was translated regarding the delay between the estimated and exact solution, matching the oscillation behavior. As expected, with a lower measurement standard deviation, the estimation reaches better results when compared to higher σ_{meas}. When the measurements standard deviation is 0.01 K, the RMS increases as the parameter p increases, probably due to the thermal inertia. Considering a standard deviation of $\sigma_{\text{meas}} = 0.06$ K, the same behavior, with respect to the RMS error, can be observed for $A = 4000$ W/m^2, while for $A = 2000$ W/m^2 the error stabilizes when the parameter p reaches 1.2. When the standard deviation of the measurements is equal to 0.1 K, the error reduces when $A = 2000$ W/m^2 and $p = 1.2$, while for $A = 4000$ W/m^2 it stabilizes for the higher p considered. Regarding the CGM with AO [9] the same trends can be observed: when the parameter A increases, the error increases, as well as when the value of the parameter p is raised. The errors obtained with the KF are higher when compared to ones obtained by the CGM with AO. However, this was expected, since the KF is a sequential method, while the CGM with AO is a whole domain technique. Therefore, the KF can be used in real time applications, while the CGM with AO has to wait until all measurements are available up to the time considered. Nevertheless, the KF errors are roughly three times higher than the ones of the CGM with AO, indicating a very good performance.

Fig. 4 presents the exact solution, the estimated heat flux, and the temperature residuals considering $\sigma_{\text{meas}} = 0.1$ K. We can see that the exact and estimated heat fluxes have the same behavior for all values of A and p. As a result of the thermal inertia, and the fact that it is a time marching technique, opposite to the whole domain technique used by the CGM with AO, the KF exhibits a somewhat delayed reaction compared to the exact solution. We quantified the delay difference between the exact and estimated solution as about 0.14 s for $p = 0.6$ and 0.36 s for $p = 1.2$, considering $A = 4000$ W/m^2. The same order of magnitude for these delays was observed for the cases where A was equal to 2000 W/m^2. Moreover, it can be observed that the temperature residuals increase when the frequency or amplitude parameters increase. The temperature residuals present the maximum and minimum values when the heat fluxes reach their maximum and minimum values, respectively, which is again related to the delayed KF response. However, this did not compromise the solution. The computational time required for the inverse problem solution was about 11.41 s for the KF, lower than the total time for the experiment (20 s). According to [9], the CGM with AO recovered the heat flux in about 3 min, using the same computer. It should be noticed that the time required to smooth the temperature, during the KF solution, was considered on this time estimation. Once the KF estimation was evaluated considering synthetic data, we can proceed with the estimation performance considering actual experimental data.

4.2. Experimental data

The experimental setup of reference [8] concerns a multi-turn aluminum PHP with 14 tubes. The experiment was performed during parabolic flights to emulate microgravity conditions, a crucial point for PHPs applications in aerospace. The device was 50 % filled with FC −72, the tubes had an inner diameter of 3 mm and an outer diameter of 5 mm, and the section studied was 84 mm long. The PHP channels were coated

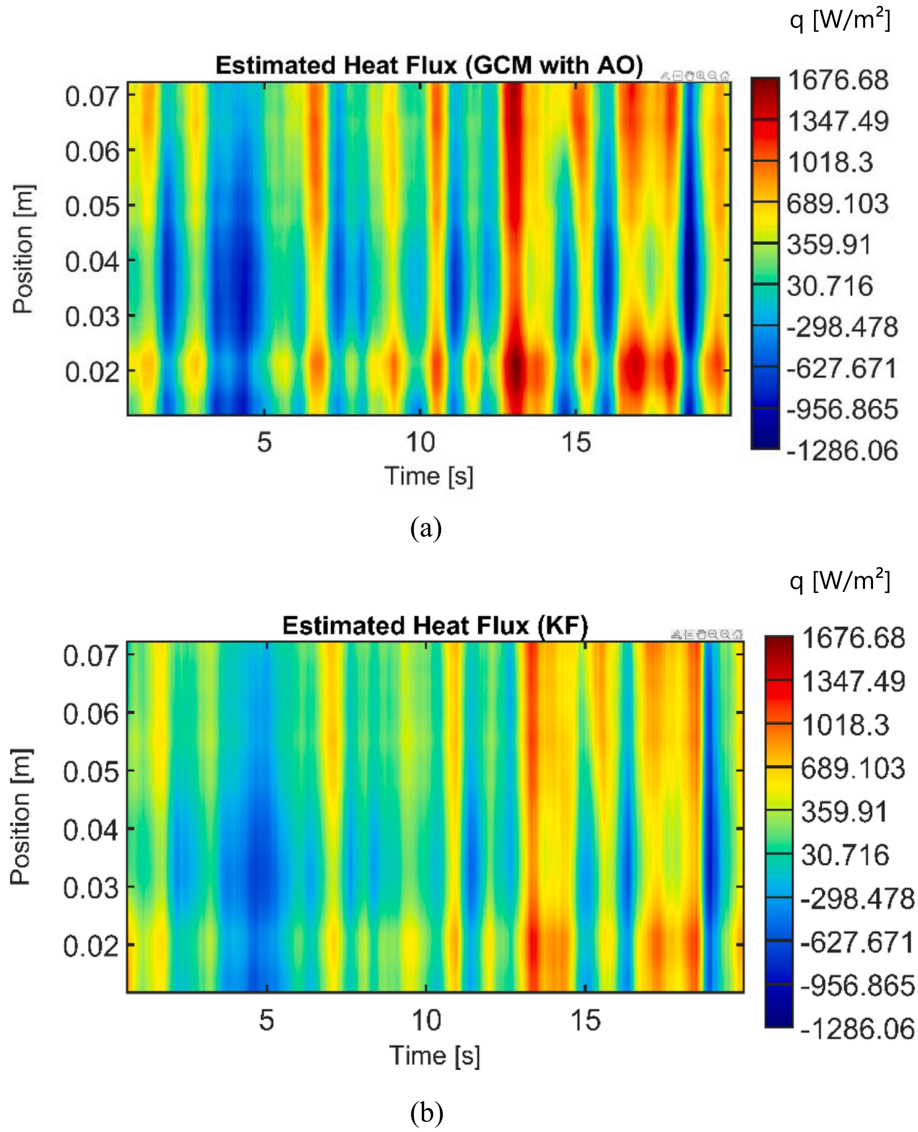

Fig. 5. Estimated heat flux by the CGM with AO [9] and the KF for a real experiment.

with black opaque paint with high emissivity. The heat was provided by a controllable power supply on the evaporator section, and a high-speed and high-resolution infrared camera recorded the temperature along the adiabatic section.

The heat flux estimates obtained by the CGM with AO [9] and the KF are shown in Fig. 5a and 5b, respectively. As discussed before, the CGM with AO is a whole domain technique. Consequently, its results are theoretically closer to the real heat flux once they use more information to obtain the entire heat flux profile. Therefore, we used them as a reference to evaluate the KF estimation. As in [9], for both boundaries, i.e., $z = 0$ and L, the results were strongly compromised, and we discarded a portion of 4.2 mm on both sides of the estimation. As we can see, qualitatively the magnitude and behavior of the internal heat fluxes obtained by the KF were close to the ones obtained with the CGM with AO. To evaluate the estimation error quantitatively, the results with the CGM with AO [9] were considered to be the exact solution in Eq. (23). Considering the amplitude parameter $A = 2000$ W/m^2, the estimation error when comparing the results obtained with the KF with the ones from the CGM with AO resulted in a deviation between the solutions of 25.5 %, which is very good for this real experimental test case. The main advantage of the proposed methodology is its simplicity of implementation and also its memory consumption, once the KF requires only the temperature measurement at each time step, instead of all time domain as performed with GCM with AO.

5. Conclusions

The goal of the current paper was the evaluation of the KF for local heat flux estimation on the internal wall of the adiabatic section of PHPs. The estimation procedure was based on the solution of an inverse heat conduction problem considering available the temperature measurement on the external wall of the pipe, obtained by an infrared camera. In order to speed-up the computational time, a mathematical manipulation during the prediction step was performed to reduce the number of matrices multiplications. The technique was first analyzed considering synthetic data, providing good results in accordance with the exact solution. Then, a real experimental test-case was considered, for a PHP operating under microgravity condition according to the reference [8]. In this sense, the KF results were compared with the CGM with AO [9], showing good agreement. In all cases, the computing time was lower than the experimental time. The estimation obtained from a whole-domain technique (CGM with AO) are better, but the main advantages of the sequential estimation of the KF are its low computational cost and simplicity of implementation, besides the low requirements of computational memory. For the synthetic case, the experiment took 20 s and the KF estimate (considering all calculations) required about 11.41 s on an Apple Silicon M1 Chip. Therefore, such technique might be applicable for real-time application, possibly on some embarked devices. Thus, the KF could be used to monitoring PHP systems, allowing the control of their operation condition and eventually emergency interruption to avoid the system failure.

CRediT authorship contribution statement

Bruno H.M. Margotto: Formal analysis, Investigation, Software, Writing – original draft. **Carlos E.P. Kopperschmidt:** Investigation. **Marcelo J. Colaço:** . **Wellington B. da Silva:** Supervision, Writing – review & editing, Investigation. **Fabio Bozzoli:** Conceptualization, Investigation, Project administration, Supervision, Writing – review & editing. **Luca Cattani:** Investigation, Writing – review & editing. **Luca Pagliarini:** Investigation, Writing – review & editing.

Declaration of competing interest

The authors declare that they have no known competing financial interests or personal relationships that could have appeared to influence the work reported in this paper.

Data availability

Data will be made available on request.

Acknowledgements

This paper was partially funded by the following Brazilian agencies: CNPq (*Conselho Nacional para o Desenvolvimento Científico e Tecnológico*), FAPERJ (Rio de Janeiro State Agency for Research), ANP-PRH8.1 (Brazilian National Agency for Oil, Gas and BioFuels – Human Research Program number 8) and CAPES (*Coordenação de Aperfeiçoamento de Pessoal de Nível Superior* – Finance Code 001). The financial support and hospitality offered by Università degli Studi di Parma was also fundamental to this research.

Appendix I

In this appendix we present the pseudo-code to build the matrix generated with Finite Difference Method used on the KF. The matrix $\mathbf{F}_{\mathrm{fdm}}$ initiates as a zero matrix with dimension of N_rN_z x N_rN_z and then the following procedure can be performed:

```
ii = 1
do i = 1, N_r
  do j = 1, N_z
    if (i == 1) then
      F_fdm(ii, ii) = 1 - 2r_r - 2r_z
      F_fdm(ii, ii + nz) = r_r
      if (j == 1) then
        F_fdm(ii, ii + 1) = 2r_z
      else if (j == N_z) then
        F_fdm(ii, ii - 1) = 2r_z
      else
        F_fdm(ii, ii + 1) = r_z
        F_fdm(ii, ii - 1) = r_z
      end if
    else if (i == N_r) then
      F_fdm(ii, ii) = 1 - 2r_r - 2r_z - (2h_∞Δr/λ)(αΔt/(2r_ext Δr) + r_r)
      F_fdm(ii, ii - N_z) = 2r_r
      if (j == 1) then
        F_fdm(ii, ii + 1) = 2r_z
      else if (j == N_z) then
        F_fdm(ii, ii - 1) = 2r_z
      else
        F_fdm(ii, ii + 1) = r_z
        F_fdm(ii, ii - 1) = r_z
      end if
    else
      F_fdm(ii, ii) = 1 - 2r_r - 2r_z
      F_fdm(ii, ii + N_z) = αΔt/(2r_i Δr) + r_r
      F_fdm(ii, ii + N_z) = -αΔt/(2r_i Δr) + r_r
      if (j == 1) then
        F_fdm(ii, ii + 1) = 2r_z
      else if (j == N_z) then
        F_fdm(ii, ii - 1) = 2r_z
      else
        F_fdm(ii, ii + 1) = r_z
        F_fdm(ii, ii - 1) = r_z
      end if
    end if
    ii = ii + 1
  end do
end do
```

References

[1] D. Bastakoti, H. Zhang, D. Li, W. Cai, F. Li, An overview on the developing trend of pulsating heat pipe and its performance, Appl. Therm. Eng. 141 (2018) 305–322.
[2] M. Marengo, V.S. Nikolayev, Pulsating heat pipes: experimental analysis, design and applications, Chapter 1, World Sci. (2018) 1–62.
[3] M. Mameli, G. Besagni, P.K. Bansal, C.N. Markides, Innovations in pulsating heat pipes: from origins to future perspectives, Appl. Therm. Eng. 203 (2022) 117921.
[4] X. Han, X. Wang, H. Zheng, X. Xu, G. Chen, Review of the development of pulsating heat pipe for heat dissipation, Renew. Sustain. Energy Rev. 59 (2016) 692–709.
[5] V.K. Karthikeyan, K. Ramachandran, B.C. Pillai, A. Brusly Solomon, Understanding thermo–fluidic characteristics of a glass tube closed loop pulsating heat pipe: flow patterns and fluid oscillations, Heat Mass Transf. 51 (2015) 1669–1680.
[6] Z. Su, Y. Hu, S. Zheng, T. Wu, K. Liu, M. Zhu, J. Huang, Recent advances in visualization of pulsating heat pipes: a review, Appl. Therm. Eng. 221 (2022) 119867.
[7] L. Cattani, D. Mangini, F. Bozzoli, L. Pietransanta, N. Miche, M. Mameli, S. Filippeschi, S. Rainieri, M. Marengo, An original look into pulsating heat pipes: inverse heat conduction approach for assessing the thermal behaviour, Therm. Sci. Eng. Progr. 10 (2019) 317–326.
[8] L. Pagliarini, L. Cattani, F. Bozzoli, M. Mameli, S. Filippeschi, S. Rainieri, M. Marengo, Thermal characterization of a multi-turn pulsating heat pipe in microgravity conditions: statistical approach to the local wall-to-fluid heat flux, Int. J. Heat Mass Transf. 169 (2021) 120930.
[9] M.J. Colaço, F. Bozzoli, L. Cattani, L. Pagliarini, Local heat flux estimation inside tubes through conjugate gradient method with adjoint operator: Application to the pulsating heat pipes case, Int. J. Numer. Meth. Heat Fluid Flow (2022), https://doi.org/10.1108/HFF-09-2022-0547.
[10] L. Pagliarini, L. Cattani, M. Mameli, S. Filippeschi, F. Bozzoli, S. Rainieri, Global and local heat transfer behaviour of a three-dimensional pulsating heat pipe: combined effect of the heat load, orientation and condenser temperature, Appl. Therm. Eng. 195 (2021) 117144.
[11] N. Iwata, F. Bozzoli, L. Pagliarini, L. Cattani, P. Vocale, M. Malavasi, S. Rainieri, Characterization of thermal behavior of a micro pulsating heat pipe by local heat transfer investigation, Int. J. Heat Mass Transf. 196 (2022) 123203.
[12] R. Doraiswami, L. Cheded, Robust model-based soft sensor: Design and application. Proceedings of the 19th World Congress the International Federation of Automatic Control Cape Town, South Africa, 2014.
[13] J.V. Beck, B. Blackwell, C.R. St. Clair Jr., Inverse Heat Conduction: Ill-Posed Problems, James Beck, 1985.
[14] B. Ristic, S. Arulampalam, N. Gordon, Beyond the Kalman Filter: Particle Filters for Tracking Applications, Artech House, 2004.
[15] J. Kaipio and E. Somersalo, Statistical and Computational Inverse Problems, Applied Mathematical Sciences, Springer, vol. 160, 2004.
[16] C. Ji, P. Tuan, H. Jang, A recursive least-squares algorithm for on-line 1-D inverse heat conduction estimation, Int. J. Heat Mass Transf. 40 (9) (1996) 2081–2096.
[17] P. Tuan, C. Ji, L. Fong, W. Huang, An input estimation approach to on-line two-dimensional inverse heat conduction problem, Numer. Heat Transfer, Part B 29 (1996) 345–363.
[18] P. Tuan, S. Lee, W. Hou, An efficient on-line thermal input estimation method using Kalman filter and recursive Least Square algorithm, Inverse Prob. Eng. 5 (1997) 309–333.
[19] P. Tuan, L. Fong, W. Huang, Application of Kalman filtering with input estimation technique to on-line cylindrical inverse heat conduction problems, Japan Soc. Mech. Eng. Int. J., Series B 40 (1997) 1.
[20] J.-H. Noh, D.-B. Kwak, K.-B. Kim, K.-U. Cha, S.-J. Yook, Inverse heat conduction modeling to predict heat flux in a hollow cylindrical tube having irregular cross-sections, Appl. Therm. Eng. 128 (2018) 1310–1321.
[21] C. Ji, H. Jang, Experimental investigation in inverse heat conduction problem, Numer. Heat Transf., Part A: Appl. 34 (1) (1997) 75–91.
[22] W. Lee, Y. Ko, C. Ji, A study of an inverse method for the estimation of impulsive heat flux, J. Franklin Inst., Elsevier Science Ltd 337 (2000) 661–671.
[23] P. Tuan, M. Ju, The validation of the robust input estimation approach to two-dimensional inverse heat conduction problems, Numer. Heat Transfer, Part B 37 (2000) 247–265.
[24] K.Y. Kim, B.S. Kim, H.C. Kim, M.C. Kim, K.J. Lee, B.J. Chung, S. Kim, Inverse estimation of time-dependent boundary heat flux with an adaptive input estimator, Int. Commun. Heat Mass Transfer 30 (4) (2003) 475–484.
[25] T. Chen, S. Hsu, Input estimation method in the use of electronic device temperature prediction and heat flux inverse estimation, Numer. Heat Transfer, Part A 52 (2007) 795–815.
[26] S. Wen, H. Qi, X. Yu, Y. Ren, L. Wei, L. Ruan, Real-time estimation of time-dependent imposed heat flux in graded index media by KF-RLSE algorithm, Appl. Therm. Eng. 150 (2019) 1–10.
[27] N. Daouas, M. Radhouani, Version étendue du filtre de Kalman discret appliquée à un problème inverse de conduction de chaleur non linéaire, Int. J. Therm. Sci. 39 (2) (2000) 191–212.
[28] H. R. B. Orlande, M. J. Colaço, G.S. Dulikravich, F. L. V. Vianna, W. B. Silva, H. M. Fonseca and O. Fudym. Kalman and Particle filters, in: METTI V - Thermal Measurements and Inverse Techniques, 2011, Roscoff. METTI V - Thermal Measurements and Inverse Techniques, 2011.
[29] C.C. Pacheco, H.R.B. Orlande, M.J. Colaço, G.S. Dulikravich, Identification of a position and time dependent heat flux using the kalman filter and improved lumped analysis in heat conduction. 5th International Conference on Computational Methods (ICCM2014). Cambridge, England, 2014.
[30] H. Qi, S. Wen, Y. Wang, Y. Ren, L. Wen, L. Ruan, Real-time reconstruction of the time-dependent heat flux and temperature distribution in participating media by using the Kalman filtering technique, Appl. Therm. Eng. 157 (2019) 113667.
[31] M.N. Ozisik, H.R.B. Orlande, M.J. Colaço, R.M. Cotta, Finite Difference Methods in Heat Transfer, CRC Press, Taylor & Francis Group, 2017.
[32] O.M. Alifanov, Inverse heat transfer problems. 1st Edition. International Series in Heat and Mass Transfer, Springer, Berlin, Heidelberg, 1994.
[33] J. Kaipio, E. Somersalo, Statistical inverse problems: discretization, model reduction and inverse crimes, J. Comput. Appl. Math. 198 (2007) 493–504.
[34] Algorithm 642: A fast procedure for calculating minimum cross-validation cubic smoothing splines, ACM Transactions on Mathematical Software, Vol. 12, Issue 2, pp 150–153, 1986.